

AESJ-KNS Joint Workshop on Reactor Physics and Nuclear Data

Kinki University, Osaka, Japan, March 25, 2013

- 12:30 - 13:00 Registration at multi-purpose room, 2nd floor, Building No. 38,
Kinki University, Higashi-Osaka Campus
- 13:00 - 13:05 Opening Speech,
Kenji Ishibashi (Chairperson, Nuclear Data Division of AESJ)
- Session I: Session chair, Tokio Fukahori (Japan Atomic Energy Agency)**
- 13:05 - 13:30 Y. Iwamoto (Japan Atomic Energy Agency),
Radiation Damage Calculation in PHITS for Materials Irradiated with
Neutrons, Protons and Deuterons over a Wide Energy Range
- 13:30 - 13:55 Chang Je Park (Korea Atomic Energy Research Institute),
A Study on the Photoneutron Effect for a Small Research Reactor
- 13:55 - 14:20 A. Kimura (Japan Atomic Energy Agency),
Neutron Capture Cross Section Measurements for Radio Isotopes using the
ANNRI in J-PARC/MLF
- 14:20 - 14:30 Coffee break
- Session II: Session chair, Deokjung Lee (UNIST)**
- 14:30 - 14:55 Han Gyu Joo (Seoul National University),
Investigation of Intra-pellet Power Profile Effects on Whole Core Transport
Calculation for Power Reactors
- 14:55 - 15:20 Yuichiro Ban (Toshiba Corporation),
The Small Reactivity Worth Measurement in Critical Experiments
- Uncertainty estimation for reactivity fluctuation -
- 15:20 - 15:45 Myung-Hyun Kim (Kyung Hee University),
A Neutronic Design of a Hybrid Reactor for Waste Transmutation
- 15:45 - 15:55 Coffee break

Session III:	Session chair, Tomohiro Endo (Nagoya University)
15:55 - 16:20	Nam Zin Cho (Korea Advanced Institute of Science and Technology), Two Formulations of Continuous-Energy Monte Carlo Local Problem in Overlapping Local/Global Iteration Methodology
16:20 - 16:45	Masato Tabuchi (Nuclear Engineering Ltd.), Efficient Calculation Scheme with Preservation of Transmission Probabilities in the Method of Characteristics
16:45 - 17:10	Deokjung Lee (Ulsan National Institute of Science and Technology) Hybrid Method of MOC and MC for Efficient Neutron Transport Analysis
17:10 - 17:15	Closing Speech, Nam Zin Cho (Korea Advanced Institute of Science and Technology)

Radiation Damage Calculation in PHITS for Materials Irradiated with Neutrons, Protons and Deuterons over a Wide Energy Range

Y. Iwamoto^{a*}, H. Iwamoto^a, M. Harada^a, K. Niita^b, T. Sawai^a

^aJapan Atomic Energy Agency, 2-4, Shirakatashirane, Tokai, Naka, Ibaraki 319-1195, Japan

^bResearch Organization for Information Science and Technology, Tokai, Naka, Ibaraki 319-1196, Japan

*Corresponding author: iwamoto.yosuke@jaea.go.jp

1. Introduction

Currently, in the design phase, there are new material irradiation facilities such as the ADS Target Test Facility (TEF-T) [1] at J-PARC and the International Fusion Materials Irradiation Facility (IFMIF). To evaluate radiation damage for the structural materials, historically, displacement per atom (DPA) is used as the unit of displacement damage intensity.

Recently, we have developed a calculation method of the displacement cross-sections [2] in the energy range from 10^{-10} MeV to 3 GeV, including event generator and Coulomb scattering in the Particle and Heavy Ion Transport code System (PHITS) [3]. For the design of facilities, the database of displacement cross-sections has been required. Although the database for J-PARC facilities was developed [4], there is no data for protons below 20 MeV and for deuteron at all energies due to a lack of Coulomb scattering model. Neutron data is not sufficient to estimate the radiation damage of the structural materials.

In this work, the authors developed the database of displacement cross-sections in the energy range from 10^{-10} MeV to 3 GeV for neutron and from 100 keV to 3 GeV for proton and deuteron using the new PHITS. It includes 14 elemental targets, many of which are common structural materials at accelerator and reactor facilities, as listed below:

${}^6\text{C}$, ${}^{27}\text{Al}$, ${}^{14}\text{Si}$, ${}^{23}\text{V}$, ${}^{24}\text{Cr}$, ${}^{25}\text{Mn}$, ${}^{26}\text{Fe}$, ${}^{28}\text{Ni}$, ${}^{29}\text{Cu}$, ${}^{41}\text{Nb}$, ${}^{42}\text{Mo}$, ${}^{74}\text{W}$, ${}^{82}\text{Pb}$, ${}^{83}\text{Bi}$

The effect of the newly calculated cross-sections in assessing radiation damage at a TEF-T target vessel and a test irradiation in IFMIF materials is illustrated in the presentation as well.

2. Radiation Damage Calculation in PHITS

Figure 1 shows overview of radiation damage calculation in PHITS. For all incident particles, Primary Knock on Atoms (PKAs) and secondary particles are created by the nuclear elastic scattering and nuclear reactions. The conservation law on the energy and the momentum is sustained in each event using nuclear reactions, INCL4.6 [5], for high energy particles with energies above 10 MeV and the event generator mode [6] for low energy neutrons below 10 MeV. These models can generate the energy distribution of the secondary particles which affect the radiation damage

calculations. These particles cause the cascade damage in a material via Coulomb scattering with a target atom. For incidence of charged particles, Coulomb scattering between incident particles and the target atom also causes the cascade damage. The conditions of various irradiations will be described by using the damage energy to characterize the displacement cascade. This is defined as the initial energy of target PKA or secondary particles created by nuclear reactions, corrected for the energy lost to electronic excitations by all of the particles composing the cascade. The point defects and their clusters affect the macroscopic material properties, such as hardness.

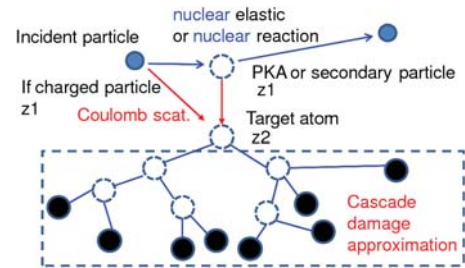


Fig. 1. Overview of radiation damage calculations in PHITS.

Displacement cross-section is calculated with Coulomb scattering using the following equation [2]:

$$\sigma = \int_{td}^{\max} \frac{d\sigma_{sc}}{dt} \eta N_{\text{NRT}} dt \quad (1)$$

where N_{NRT} is the number of defects produced in irradiated material. σ_{sc} is a universal one-parameter differential scattering cross-section equation in reduced notation. η is the defect production efficiency (number of survived defects to NRT predictions) [7] introduced by C.H.M. Broeders et al. They have shown that the NRT model overestimates the number of displacements. The authors therefore made database of displacement cross-sections in addition to defect production efficiency for ${}^{26}\text{Fe}$, ${}^{29}\text{Cu}$ and ${}^{74}\text{W}$ listed in the paper [7].

3. Calculated Displacement Cross-Sections

Figure 2 shows the displacement cross-sections for copper irradiated with proton, neutron or deuteron versus incident energy in the energy range from 0.1 MeV to 3 GeV. The defect production efficiency, η , was 1 for σ_{NRT} curves. For $\sigma_{\text{BCA-MD}}$, η was obtained from the paper [7]. For protons and deuterons at energies above 20 MeV, the secondary particles created by nuclear reaction are more dominant than PKAs

produced by nuclear elastic scattering, and contribution of Coulomb scattering for the secondary particles increases with energy. For the proton-induced cross-sections below 20 MeV, the PHITS results are in good agreement with the experimental data. In the all cases, the difference between $\sigma_{\text{BCA-MD}}$ and σ_{NRT} increases with energies. For neutrons at 14 MeV, protons at 1.1 GeV and 1.94 GeV, the agreement between $\sigma_{\text{BCA-MD}}$ and the experimental data is better than the agreement between σ_{NRT} and data [2]. For deuterons, we found that displacement cross-sections above 20 MeV, which is mainly produced by the secondary particle, give good agreement with the data for proton and neutron within a factor of 1.5. Finally, σ_{NRT} for the 14 elemental targets as listed in '1. Introduction' and $\sigma_{\text{BCA-MD}}$ for ^{26}Fe , ^{29}Cu and ^{74}W were obtained by using the radiation damage calculation. The cross-sections were folded into calculated particle fluxes in PHITS to estimate DPA values.

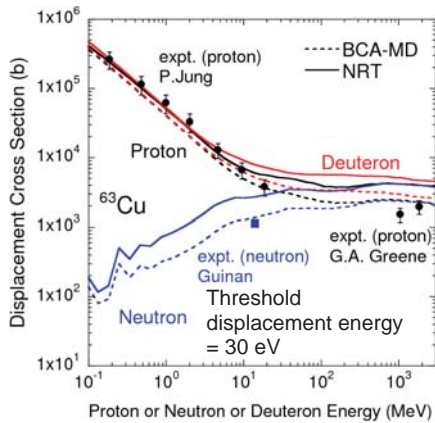


Fig. 2. The displacement cross-sections of copper as a function of incident neutron, proton or deuteron energy. $\eta=1$ for solid lines and η =equation in ref. [7] for dashed lines. The experimental data summarized in ref. [2] are also shown.

4. Displacement Production due to Protons at TEF-T and Deuterons at IFMIF

In this section, applications of the calculated displacement cross-sections, σ_{NRT} , to the radiation damage calculations at TEF-T and IFMIF are described. At TEF-T, 400 MeV protons were irradiated with the SUS316 specimen (compositions used in the calculations given in atomic %: 67.4Fe-18.4Cr-11.5Si-1.5Mo-1Mn-0.2C, size: 0.2 cm \times 4 cm \times 15 cm), which was contained within the spallation target of lead-bismuth eutectic (LBE). For deuteron-irradiation test, 40 MeV deuteron beam was employed and the SUS316 specimen was contained within air. Figure 3 shows the depth dependence of the DPA value for 400 MeV-250 kW proton into SUS316+LBE with 4,500 hours irradiation and 40 MeV-10 MW deuteron into SUS316 with 10 hours.

occur before the stopping range is reached, and secondary particles contribute to the overall DPA value at target depths below the range.

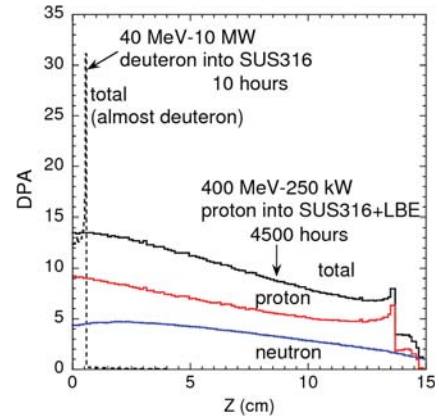


Fig. 3. The depth dependence of DPA for SUS316 specimen irradiated by 400 MeV proton and 40 MeV deuteron beams.

5. Conclusions

The displacement cross-sections for common structural materials were calculated using the radiation damage calculation method in PHITS. The displacement cross-sections with the defect production efficiency gave good agreement with experimental data. For application to the DPA calculations at 400 MeV proton and 40 MeV deuteron, calculated cross-sections were folded into calculated particle fluxes in PHITS. Thus the PHITS including the displacement cross-sections can be useful to calculate the DPA values in materials used at accelerator facilities that will be exposed to intense primary and secondary particle irradiation. It will also be useful at fission and fusion reactor facilities.

REFERENCES

- [1] S. Saito, Pb-Bi Target Development at JAEA, The 10th International Workshop on Asian Network for Accelerator-Driven System (ADS) and Nuclear Transmutation Technology (NTT), 6th and 7th December, 2012, at KURRI, Japan.
- [2] Y. Iwamoto, K. Niita, T. Sawai et al., Improvement of Radiation Damage Calculation in PHITS and Tests for Copper and Tungsten Irradiated with Protons and Heavy-ions over A Wide Energy Range, Nuclear Instruments and Methods In Physics Research B, Vol.274, p.57, 2012.
- [3] K. Niita et al., PHITS: Particle and Heavy Ion Transport Code System, Ver. 2.23, JAEA-Data/Code, 2010-022, 2010.
- [4] M. Harada, N. Watanabe, C. Konno et al., DPA Calculation for Japanese Spallation Neutron Source, Journal of Nuclear Materials, Vol.343, p.197, 2005.
- [5] A. Boudard, J. Cugnon, J.-C. David, S. Leray, and D. Mancusi, New Potentialities of the Liège Intranuclear Cascade Model for Reactions Induced by Nucleons and Light Charged Particles, Physical Review C, Vol.87, 014606, 2013.
- [6] Y. Iwamoto, K. Niita, Y. Sakamoto et al., Validation of the Event Generator Mode in The PHITS Code and Its

Application, International Conference on Nuclear Data for Science and Technology 2007, DOI: 10.1051/ndata:07417.

[7] C.H.M. Broeders and A.Yu. Konobeyev, Defect Production Efficiency in Metals under Neutron Irradiation, Journal of Nuclear Materials, Vol.328, p. 197, 2004.

A Study on the Photoneutron Effect for a Small Research Reactor

Chang Je Park* and Byungchul Lee

Korea Atomic Energy Research Institute, 1045 Daedeok-daero, Yuseong-gu, Daejeon, 305-353, Korea

*Corresponding author: cjpark@kaeri.re.kr

1. Introduction

A small research reactor has been designed to provide high neutron flux toward the beam tube for cold neutron beam research based on the HOR reactor.[1] Total 9 square fuel assemblies are loaded. In order to manage fuel assembly easily, a single square type of fuel assembly is proposed in this design. Beryllium is chosen as the reflector, which provides a better characteristics of neutron moderation. However, the photoneutron effect of Be should be scrutinized especially for kinetics parameter and decay heat after shutdown. In order to control the reactor safely, the kinetics parameter such as delayed neutron yield and the neutron generation time are very important.[2] And the decay heat and neutron source after shutdown play an important role to manage the reactor and to restart the reactor, too.[3] In this study, the photoneutron effect of Be reflector is analyzed with three different computer code systems. The equilibrium core is searched by the McCARD code [4] and the depletion analysis of fuel assembly has been done with the ORIGEN-S code[5], from which the gamma intensities are used as the source term to estimate photoneutron in the Be reflector by using the MCNP5 code[6].

In Section 2, the core configuration of the small research reactor is provided. And calculation model and results are described in Section 3. Finally, Section 4 provides conclusions of this study.

2. Core Configuration of Small Research Reactor

The small research reactor is simply designed to enhance the thermal neutron flux at the nose of the beam tube for cold neutron beam research by shifting fuel assemblies toward the beam tube as shown in Fig. 1. The core fission power is 3 MW and the reflector is Be square block which size is 81 mm x 81 mm. The core composed of 5 standard fuel assemblies and 4 control fuel assemblies. The fuel is a typical plate type and both the standard fuel assembly and the control fuel assembly are all the same size in a square shape. The composition of fuel meat is U_3Si_2 -Al and its enrichment of uranium is 19.75 wt% U-235, which is a typical value in current research reactors. As an alternative, UMo-Al fuel is also taken into consideration, which provides more uranium density and longer fuel cycle. The specification of the fuel assembly is given in Table I. Due to a single type of fuel assembly, it is a great advantage in fuel management for flexible core configuration. The control fuel assembly is surrounded

by a square control plate. The thickness of control absorber is 3 mm and the height is 650 mm. In the reference core, the Hf metal is chosen as the control absorber and it provides enough reactivity worth to ensure a safe shutdown of reactor.

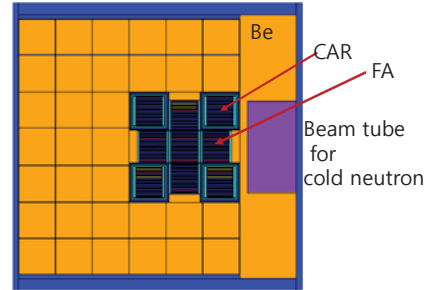


Figure 1. Core configuration of the small research reactor

Table I. Fuel Data for the Small Research Reactor

Item	Value
Fuel Meat Material	U_3Si_2 -Al UMo-Al
U density (g/cc)	4.8 : U_3Si_2 8.0 : UMo
Meat thickness (mm)	0.76
Meat width of standard FA(mm)	63.2
Cladding thickness (mm)	0.38
Moderator channel thickness (mm)	2.46
Number of plates in standard FA	20
FA size (mm)	81x81x600

3. Analysis Results of Photoneutron Effect

In order to analyze photoneutron effect in Be reflector, as a first step, a core depletion calculation is carried out to find an equilibrium core by the McCARD code. Two types of fuels are used with different fuel cycle lengths. In the case of U_3Si_2 fuel, 70 days per cycle is given and the UMo fuel takes 150 days per cycle. The estimated discharge burnups are about 44 %U-235 and 54 %U-235 for U_3Si_2 fuel and UMo fuel, respectively, which are provided in Fig. 2. From the burnup data, the gamma source term is obtained up to 3 days from the ORIGEN-S calculation for 9 different assemblies. By using total gamma intensities in the core after shutdown, the photoneutron in the Be reflector is calculated with the MCNP5 code. The ENDF7u library is used to consider photoneutron effect. The obtained total gamma intensity of the fuel region and the average photoneutron flux in reflector region are tabulated in Table II. Photoneutrons in Be reflector

of U_3Si_2 fuel loaded core varies from $5.4E+10$ n/cm²s to $3.5E+8$ n/cm²s as the time passes from 1 s to 3 days. The photoneutron fluxes of UMo loaded core are similar to those of U_3Si_2 loaded core due to similar gamma spectra. Decay heat of Be reflector after shutdown is also estimated from the results of the photoneutron flux calculation. The ORIGEN-S code is used with the flux irradiation option and Fig. 3 shows the distribution of decay heat as a function of time after shutdown. The decay heats in Be reflector region of two different cores are similar and as the shutdown time increases, the decay heat decreases from about $3E-05$ W/cc to $3E-07$ W/cc.

The kinetic parameter is also estimated by the same way as proposed in Ref.[2] The MCNP5 code is used and it is assumed that the U_3Si_2 fuel is fresh with a single fuel density. The gamma rays producing photoneutrons are produced from prompt and delayed fission gammas, prompt and delayed capture gammas. Ignoring delayed gammas, the effective delayed neutron fission fraction can be estimated by the coupled neutron-photon calculation in MCNP5 code using mpn card for the reflector materials only. From the simulation, the delayed fractions of photoneutron from prompt fission gamma and prompt capture gamma is estimated 0.00028, 0.00024 for U_3Si_2 and UMo fuels, respectively, which are similar results compared with that of Ref.[2]. The corresponding ratios to the effective delayed neutron fraction are about 3.8%, 3.4% for U_3Si_2 and UMo fuels, respectively.

CA1	FA1	CA2	FA ID	CA1	FA1	CA2	FA ID
22.5	11.6	36.9		BOC	28.7	14.9	
27.8	17.2	40.8	EOC	35.3	22.0	50.6	EOC
FA2	FA3	FA4	FA ID	FA2	FA3	FA4	FA ID
5.6	40.8	0.0		BOC	7.0	50.6	
11.6	44.4	5.6	EOC	14.9	54.4	7.0	EOC
CA3	FA5	CA4	FA ID	CA3	FA5	CA4	FA ID
32.2	17.2	27.8		BOC	40.6	22.0	
36.9	22.5	32.2	EOC	46.1	28.7	40.6	EOC

U_3Si_2 (70 days/cycle) UMo (150 days/cycle)

Figure 2. Burnup of the small research reactor at the equilibrium core (%U-235)

4. Conclusions

In this study, the small research reactor is suggested with two types of fuels, U_3Si_2 and UMo. From the depletion calculation, the equilibrium core is searched and some reactor parameters are obtained including the discharge burnup. By use of burnup data of each assembly, the photoneutron effect in Be reflector has been investigated through two code systems, the ORIGEN-S and the MCNP5 code systems. Among several important parameters to be checked, it is obtained decay heat after shutdown and delayed neutron fraction in this study. For two types of fuels, the similar decay heats are estimated and the absolute level is low as expected. The delayed neutron fraction due to photoneutron is also obtained based on the previous approaches and there is not so large difference from the reference. These photoneutron data will be utilize as an

major input for the safety analysis and for the restart analysis after reactor shutdown.

As a further work, a detail study on the core design data will be performed by analyzing the reactivity feedback coefficient and neutron detector response.

REFERENCES

- [1] H. Gibcus, P.D. Leege, F. Labohm, J. D. Vries, A. Verkooijen, J. Valko, W. Feltes, and J. Heinecke, "Options for the Delft Advanced Neutron Source", IGORR 2003 – the 9th Meeting of the International Groups on Research Reactors, March 2003, Sydney, Australia (2003).
- [2] B. Dionne and N. Hana, "Impact of Photoneutrons on Transients for the MURR and MITR HEU and LEU Cores", RERTR 2010 – the 32nd International Meeting on Reduced Enrichment for Research and Test Reactors, October 2010, Lisbon, Portugal (2010).
- [3] M.S. Onegin, "Delayed Photoneutrons in the PIK Reactor", Atomic Energy, Vol. 107, No.3, 194, 2009.
- [4] H.J. Shim and C.H. Kim, McCARD: Monte Carlo Code for Advanced Reactor Design and Analysis, User's Manual, Ver. 1.1, Seoul National University, 2011.
- [5] I.C. Gauld, O.W. Hermann, R.M. Westfall, ORIGEN-S: SCALE System Module to Calculate Depletion, Actinide Transmutation, Fission Product Buildup and Decay, and Associated Radiation Source Terms, ORNL/TM-2005/39, Ver.6, Vol.II, Sect. F7 (2009).
- [6] X-5 Monte Carlo Team, MCNP - A General Monte Carlo N-Particle Transport Code, Version 5, LA-CP-03-0245, Los Alamos National Laboratory (2003).

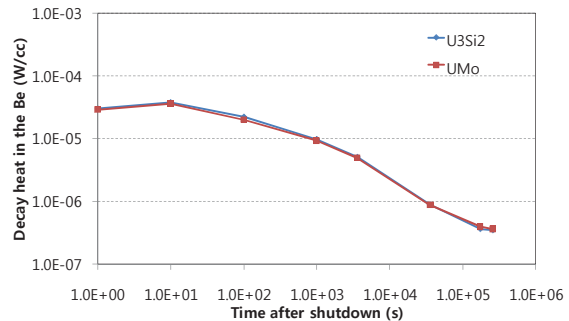


Figure 3. Decay heat in the Be reflector after shutdown

Table II. Photoneutron Flux in Be Reflector and Gamma Intensity in the Core Region

Time after shutdown	U_3Si_2		UMo	
	Avg. flux (n/cm ² s)	Gamma intensity (photon/s)	Avg. flux (n/cm ² s)	Gamma intensity (photon/s)
1 s	5.35E+10	9.41E+17	5.07E+10	9.44E+17
10 s	3.85E+10	7.89E+17	3.64E+10	7.93E+17
100 s	2.29E+10	5.81E+17	2.02E+10	5.86E+17
1000 s	9.80E+09	3.90E+17	9.37E+09	3.95E+17
1 hours	5.21E+09	2.80E+17	5.02E+09	2.86E+17
10 hours	9.07E+08	1.57E+17	8.86E+08	1.63E+17
2 days	3.69E+08	9.89E+16	4.02E+08	1.04E+17
3 days	3.52E+08	8.47E+16	3.67E+08	8.90E+16

*Relative error < 0.1

Neutron capture cross section measurements for radio isotopes using the ANNRI in J-PARC/MLF

A. Kimura^{a*}, T. Fujii^b, S. Fukutani^b, M. Furusaka^c, K. Furutaka^a, S. Goko^{a,1}, H. Harada^a, F. Hiraga^c, J. Hori^a,
M. Igashira^d, T. Kamiyama^c, T. Katabuchi^d, T. Kin^{a1}, K. Kino^c, F. Kitatani^a, Y. Kiyonagi^c, M. Koizumi^a,
M. Mizumoto^d, S. Nakamura^a, K. Takamiya^b, Y. Toh^a

^a*Nuclear Science and Engineering Directorate, Japan Atomic Energy Agency, Tokai-mura, Naka-gun, Ibaraki, 319-1195, Japan*

^b*Research Reactor Institute, Kyoto University, 2-1010, Kumatori-cho, Sennan-gun, Osaka, 590-0494, Japan*

^c*Graduate School of Engineering, Hokkaido University, Kita-ku, Sapporo, Hokkaido, 060-8628, Japan*

^d*Research Laboratory for Nuclear Reactors, Tokyo Institute of Technology, O-okayama, Meguro-ku, Tokyo, 152-8550, Japan*

Present address: ¹ *Japan Nuclear Energy Safety Organization*, ² *Kyusyu University*

^{*} *Corresponding author: kimura.atsushi04@jaea.go.jp*

1 Introduction

Accurate data of neutron-capture cross sections are important in detailed engineering designs and safety evaluations of innovative nuclear reactor systems [1-2]. Especially, neutron-capture cross sections of minor actinides (MAs) and long-lived fission products (LLFPs) have attracted attention in the field of nuclear systems such as transmutation of radioactive waste and various innovative reactor systems. However, accurate measurements of these cross sections are very difficult due to high radioactivity of these samples.

To overcome the difficulty, the Accurate Neutron-Nucleus Reaction measurement Instrument (ANNRI) has been developed by the collaboration of Hokkaido University, Tokyo Institute of Technology, and JAEA. The ANNRI is located on the Beam Line No. 04 of the materials and life science experimental facility (MLF) in the Japan Proton Accelerator Research Complex (J-PARC) [3]. A series of neutron capture cross-section measurements have been started using the ANNRI [4]. The results for ²⁴⁴ and ²⁴⁶Cm and ²³⁷Np were reported in Refs. [5] and [6]. As an example of neutron-capture cross-section measurements, a brief view of the measurements for ²⁴⁴ and ²⁴⁶Cm will be presented.

2 Experimental Procedure

The measurements of prompt γ rays emitted in the neutron-capture reactions have been performed with an array of germanium (Ge) detectors in the ANNRI.

The array of Ge detectors is composed of twenty-two Ge crystals and located on the flight length of 21.5 m as described in Ref. [4]. The pulsed neutron beam was collimated to a 7 mm diameter at the sample position. The energy-integrated neutron intensities at the sample position are 4.5×10^6 n/s/cm² in the neutron energy range of 1.5-25 meV at a beam power of 120 kW. In the experiments, J-PARC was operated at a repetition rate of 25 Hz, a power of 120 kW and in the "double-bunch mode", in which each proton pulse consists of two bunches (each with a width of 100 ns) at intervals of 600 ns.

The ²⁴⁴Cm sample for γ -ray measurements contained 0.6 mg of curium oxide. Its isotopic enrichment was 90.1 mole%, and its main activity was ²⁴⁴Cm 1.8 GBq. The ²⁴⁶Cm sample contained 2.1 mg of curium oxide. Its isotopic enrichment was 59.4 mole% with a 27.5 mole% contamination of ²⁴⁴Cm, and its main activities were ²⁴⁶Cm 12.1 MBq and ²⁴⁴Cm 1.7 GBq. To fulfill the safety regulations at MLF, each sample was sealed in an aluminum case 9 mm in outer diameter, weighing 280 mg, and having 0.5-mm-thick walls.

Each sample was put in a bag of fluorinated ethylene propylene (FEP) films and attached to a sample holder. Random timing pulses were fed into every pre-amplifier from a random pulse generator in order to make a dead-time correction. The total measuring time was about 64 hours for the ²⁴⁴Cm sample and about 94 hours for the ²⁴⁶Cm sample. For the background estimation, γ -ray measurements with an empty aluminum case and an empty FEP bag were also carried out for 48 hours and 44 hours, respectively.

3 Results and Discussion

Pulse-height spectra gated at the first resonance of ²⁴⁴Cm and ²⁴⁶Cm are shown in Fig. 1. The spectra were obtained by subtracting off-resonance spectra from on-resonance spectra. Eight and five γ -ray emissions were observed in the ²⁴⁴Cm(n, γ) and ²⁴⁶Cm(n, γ) reactions, respectively. In the spectrum for the ²⁴⁴Cm resonance, the 252- and 381-keV γ -rays have already been studied in other reactions. The other six γ -rays were not known until now. In the spectrum for the ²⁴⁶Cm resonance, all the five prompt γ -rays are previously unknown.

The dead time of the data acquisition system was corrected using the random timing pulses. The backgrounds due to scattered neutrons were estimated using the capture γ -ray yields for the empty FEP bag sample and the empty aluminum sample. Correction factors for neutron self-shielding and multiple scattering were calculated with the Monte Carlo simulation code MCNP. The neutron spectrum determined by measuring 478-keV γ -rays emitted in ¹⁰B(n, α) reactions. Relative cross sections were

deduced by using the TOF spectra, the deduced backgrounds, these corrections and the neutron spectrum. Contributions from chemical and isotopic impurities were obtained and subtracted by broadening the evaluated values of JENDL-4.0 with SAMMY[9] and by normalizing the broadened values to the relative cross sections at the strongest resonances. The cross sections for ^{244}Cm and ^{246}Cm were derived by normalizing the relative cross sections to the evaluated values in JENDL-4.0 using the resonance area of the first resonance of ^{240}Pu .

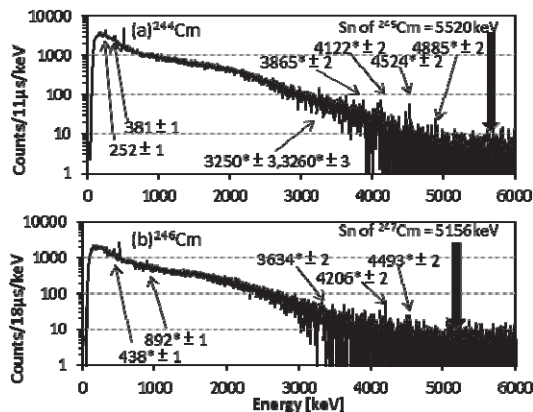


Fig. 1 The pulse-height spectra gated at the first resonance of ^{244}Cm (a) and ^{246}Cm (b). Asterisks (*) indicate previously unknown γ rays.

The obtained neutron-capture cross sections for ^{244}Cm and ^{246}Cm are shown in Fig. 2 together with those measured by Moore[10] and with JENDL-4.0 (broadened with SAMMY). The resonances of ^{244}Cm at around 7.7 and 16.8 eV and of ^{246}Cm at around 4.3 and 15.3 eV were observed in the capture reactions for the first time. The uncertainties of the obtained cross sections are 5.8% at the energy of the first resonance of ^{244}Cm and 6.6% at that of ^{246}Cm .

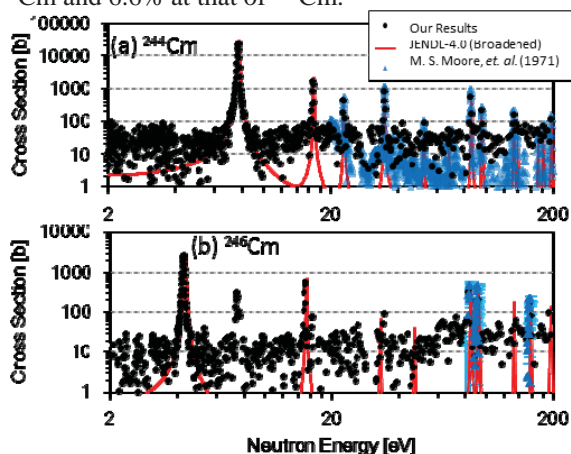


Fig. 2 Deduced neutron capture cross sections of ^{244}Cm (a) and ^{246}Cm (b) and comparison to those measured by Moore[10] and broadened JENDL-4.0[8].

4 Conclusions

The series of neutron capture cross-section measurements have been started using the ANNRI. The results gave accurate data for the neutron capture cross sections of ^{244}Cm and ^{246}Cm in the resonance region. This achievement also shows the effectiveness of the ANNRI for the measurement of neutron capture cross sections of highly radioactive samples.

The authors would like to thank the accelerator and technical staff at J-PARC for operation of the accelerators and the neutron production target and for the other experimental supports.

Present study includes the result of "Study on nuclear data by using a high intensity pulsed neutron source for advanced nuclear system" entrusted to Hokkaido University by the Ministry of Education, Culture, Sports, Science and Technology of Japan (MEXT).

This work is supported by JSPS KAKENHI (22226016 and 22760675).

REFERENCES

- [1] NEA/WPEC-26, Uncertainty and target accuracy assessment for innovative systems using recent covariance data evaluations, ISBN 978-92-64-99053-1, 2008.
- [2] G. Aliberti, G. Palmiotti, et. al., Nuclear data sensitivity, uncertainty and target accuracy assessment for future nuclear systems, *Annals of Nuclear Energy*, 33 (2006), pp. 700-733.
- [3] M. Igashira, Y. Kiyangi, et. al., Nuclear data study at J-PARC BL04, *Nucl. Instrum. Meth. Phys. Res. A*, 600 (2009), pp. 332-334.
- [4] T. Kin, K. Furutaka, et. al., Development of a 4π Germanium Spectrometer for Nuclear Data Measurements at J-PARC, the 2009 NSS-MIC Conf. Rec., Orland USA, Oct. 25-31, 2009 (2009), pp. 1194-1197.
- [5] A. Kimura, et al., Neutron-capture cross-sections of ^{244}Cm and ^{246}Cm measured with an array of large germanium detectors in the ANNRI at J-PARC/MLF, *J. Nucl. Sci. Technol.*, 49 (2012), pp. 708-724.
- [6] K. Hirose, et al., Cross-section measurement of ^{237}Np (n, γ) from 10 meV to 1 keV at Japan Proton Accelerator Research Complex, *J. Nucl. Sci. Technol.*, 50 (2013), pp. 188-200.
- [7] K. Kino, et. al, Measurement of energy spectra and spatial distributions of neutron beams provided by the ANNRI beamline for capture cross-section measurements at the J-PARC/MLF, *Nucl. Instrum. Methods. Phys. Res. A*, 626 (2011), pp. 58-66.
- [8] K. Shibata, et. al., JENDL-4.0: A New Library for Nuclear Science and Engineering, *J. Nucl. Sci. Technol.* 48 (2011), pp. 1-30.
- [9] N. M. Larson, Updated Users' Guide for SAMMY: Multilevel R-Matrix Fits to Neutron Data Using Bayes' Equations, ORNL/TM-9179/R7, Oak Ridge National Laboratory (2006).
- [10] M. S. Moore, G. A. Keyworth, Analysis of the Fission and Capture Cross Sections of the Curium Isotopes, *Physical Review C*, 3 (1971), pp. 1656-1667.

Investigation of Intra-pellet Power Profile Effects on Whole Core Transport Calculation for Power Reactors

Yeon Sang Jung and Han Gyu Joo*

Seoul National University, 1 Gwanak-ro, Gwanak-gu, Seoul 151-744, Korea
joohan@snu.ac.kr

1. Introduction

The purpose of the whole core transport calculation incorporating multi-physics phenomena which can occur in a power reactor is to attain high fidelity in the core behavior prediction. All the physical phenomena occurring in a reactor should be adequately modeled in such high fidelity realistic simulations. One of the real phenomena that can be overlooked in the whole core calculation is the nonuniform heat generation within each pellet which results from the rim effect. It is initially caused by the spatial resonance self-shielding effect that would result in edge peaked fissile Plutonium buildup production in burned pellets. In addition to the increased peripheral absorption due to the resonance self-shielding of U-238 in the region of lower temperature, the nonuniform power profile effect should be properly incorporated in the core calculation for properly representing the Doppler effect. In a previous work by Mastumoto *et al.* for the single pin-cell level calculation[1], it was confirmed that the right profile for the pellet leads to smaller power defects than the predicted values obtained with a flat profile. In this work, the effect of intra-pellet power profiles on the whole core transport calculation is investigated for an operating pressurized water reactor (PWR) with the direct whole core transport code nTRACER[2].

2. Incorporation of Intra-pellet Power Profiles in Whole Core Transport Calculations

Because of the spatial self-shielding due to U-238 resonance absorption, more fissile plutonium isotopes are built up at the periphery of a fuel pellet as the fuel depletes. This would lead to a higher heat generation rate at the rim of burned fuels as illustrated in Fig. 1. As a consequence, the interior fuel temperature is reduced while the pellet surface temperature is not much affected. Recently, the effect of the temperature profile on the effective cross sections was examined[3], but the consistent incorporation of power and temperature profiles in actual core calculations was not considered.

2.1. Fuel Conduction Calculation with Intra-pellet Power Profiles

In the fuel conduction calculation, the finite difference method with the point scheme is adopted widely. The point scheme, however, is not a conservation scheme meaning that it cannot guarantee the conservation of the energy specified as the source

term on the right hand side. This was no problem for the flat power cases, but not for the nonuniform profile cases. With this consideration, the heat conduction equation was discretized in this work with the volume scheme which can preserve the heat generation rate of each mesh explicitly. On the other hand, the temperature and burnup dependent thermal properties of UO₂ fuel pins, e.g., thermal conductivity and gap conductance, should be assigned properly by using measured data. Here the thermal conductivity correlation taken from the data for the NRC's FRAPCON 3.4 code[4] was used and the gap conductance data for typical OPR1000 fuel pins obtained from the Korean fuel vendor were used.

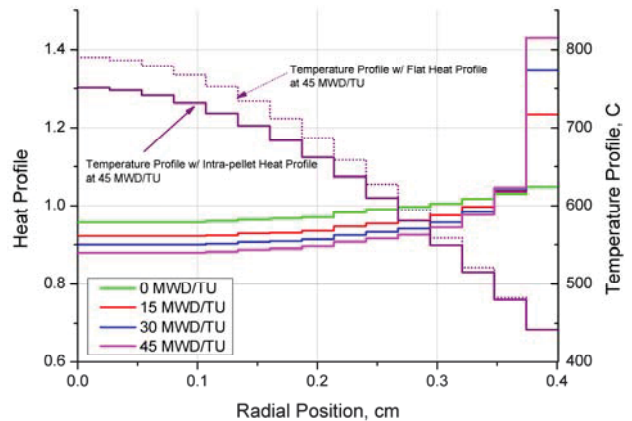


Fig. 1. Intra-pellet Power and Temperature Profiles of Burned Fuels

2.2. Resonance Self-shielding Calculation with Non-uniform temperature profiles

The temperature profile obtained from the heat conduction calculation is used in the subsequent resonance self-shielding calculation to generate effective multigroup cross sections. Here the self-shielded cross section for the resonance energy range is evaluated with the sub-group method for the direct whole core transport calculation. The limitation of the conventional subgroup method requiring a uniform temperature is mitigated by the temperature dependent subgroup formulation of nTRACER[5] where the number density of resonance isotopes is adjusted such that the resulting macroscopic cross sections can represent the temperature dependency properly in the nonuniform temperature profile cases.

3. Effects of Intra-pellet Power Profiles

In order to investigate the effects of intra-pellet power profiles, nTRACER was applied to the depletion calculation of the initial core of Yonggwang Nuclear Unit 3(YGN3C1) and to the Doppler power coefficient calculations.

3.1. Effect on OPR1000 Depletion Calculations

As shown in Fig. 2 which provides the critical boron concentration data obtained with and without the consideration of intra-pellet power profiles as well as the measured ones, essentially no difference is found between the two calculation cases. It implies that the impact of the intra-pellet power profile during the normal power operation is marginal.

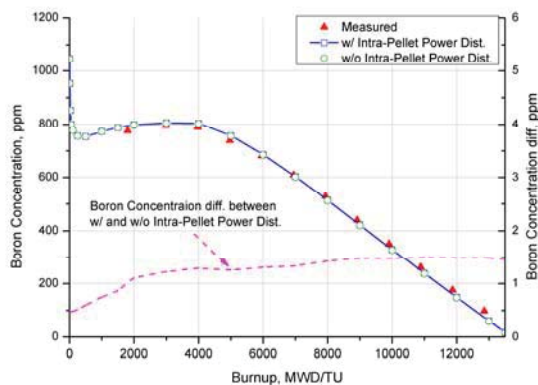


Fig. 2. Effect of Intra-Pellet Power Profile on YGN3C1 Core Depletion

3.2 Effect on Doppler Power Coefficients

The Doppler power coefficient is expected to be over-predicted (in absolute magnitude) with the flat power profile scheme because the average fuel temperature will be higher than the actual value for an edge-peaked power profile. Thus it would lead to an under-prediction of reactivity with the increasing core power level. This effect was examined for the YGN3C1 core by performing the core calculation at higher power levels as shown in Fig. 3. The coolant temperature was made unchanged by adjusting the core flow rate.

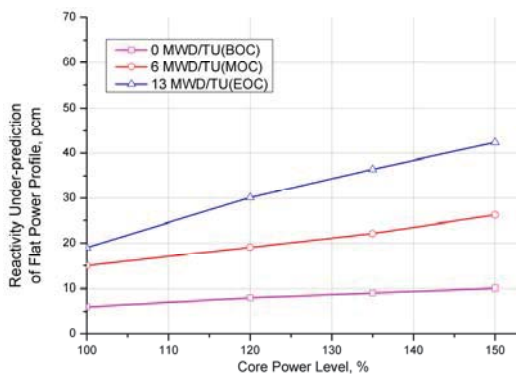


Fig. 3. Reactivity Under-prediction with Flat Power Profile in YGN3C1

Fig. 3 shows the difference in the reactivity decrement at a higher power level from the HFP condition between the two calculations. Here larger under-prediction is observed at higher burnup because of the increased rim effect with more plutonium buildup. From these results, the Doppler power coefficients were also calculated and are compared in Table 3 for the three burnup levels. The reduction in Doppler power coefficient observed at EOC1 is about 5% which is not negligible. And it will be larger in the subsequent reload cycles.

Table 1. Effect of Intra-Pellet Power Profile on Doppler Power Coefficients of YGN3C1

Burnup, MWD/TU	Doppler Power Coefficient, pcm/% power		
	IPPP ¹⁾	Flat Profile	Error, %
0	-9.44	-9.52	0.86
6	-8.36	-8.58	2.65
13	-8.52	-8.98	5.48

1) Intra-Pellet Power Profile, IPPP

4. Conclusions

The thermal feedback treatment with intra-pellet power profiles was incorporated in the direct whole core transport code nTRACER and was applied to the power reactor calculations. In the depletion calculation, only marginal effect was observed. A notable increase of about 5% is, however, observed in the Doppler power coefficient at EOC1. Since stronger effect should be observed in the following cycles where the fuel burnup is higher, estimation of the power profile effect in the reload cycles is underway.

Acknowledgement

This work was supported by MEST of Korea through NRF Grant No. 2009-0083414.

References

- [1] H. Matsumoto, M. Ouisloumen and T. Takeda, "Spatially Dependent Self-Shielding Method with Temperature Profile for Two-Dimensional Code PARAGON," *J. Nucl. Sci. Tech.*, **43**, 1311-1319, 2006.
- [2] Y.S. Jung, "nTRACER V1.0 Methodology Manual," SNURPL-CM-001(10), Seoul National University Reactor Physics Laboratory, 2010.
- [3] C.H. Lim, Y.S. Jung and H.G. Joo, "Incorporation of Resonance Up-scattering and Intra-Pellet Power Profile in Direct Whole Core Calculation," Proc. KNS Spring Meeting, Jeju, Korea, May 17-18, 2012.
- [4] K.J. Geelhood, W.G. Luscher, C.E. Beyer and M.E. Flanagan, "FRAPCON-3.3: A Computer Code for the Calculation of Steady-State, Thermal-Mechanical Behavior of Oxide Fuel Rods for High Burnup," NUREG/CR-7022, Vol.1, NRC, 2011.
- [5] Y.S. Jung, U.C. Lee, and H.G. Joo, "Examination of Temperature Dependent Subgroup Formulations in Direct Whole Core Transport Calculation for Power Reactors," Proc. ICAPP, Chicago, IL, USA, June 24-28, 2012.

The Small Reactivity Worth Measurement in Critical Experiments - Uncertainty estimation for reactivity fluctuation -

Yuichiro Ban^{a*}, Kenichi Yoshioka^b, Hironori Kumanomido^b

^a*Isogo Nuclear Engineering Center, Power Systems Company, Toshiba Corporation, 8 Shinsutita-cho, Isogo-ku, Yokohama, 235-8523*

^b*Power & Industrial Systems Reserch & Development Center, Power Systems Company, Toshiba Corporation, 4-1, Ukishima-cho, Kawasaki-ku, Kawasaki, 210-0862*

^{*}*Corresponding author: yuichiro.ban@toshiba.co.jp*

1. Introduction

A small reactivity worth measurement plays important role in reactor physics experiments. However, the measurement uncertainty of the small reactivity depends on phenomena fluctuation e.g., critical water level. The reduction of the uncertainty and the accurate estimation of the uncertainty are required.

There are several measurement methods for reactivity worth, e.g., difference of critical water level method^[1], pile oscillator method^{[2],[3]}, foil activation method^[4] and so on. Although the pile oscillator method is suitable for small reactivity measurement, it requires an expensive equipment and complex procedure to deduce reactivity from measured data.

We proposed “sample jerk method” as a robust measurement method for small reactivity worth. We have already developed a sample driving device and used for sub-criticality measurements^[5]. In order to improve the measurement uncertainty of the sample jerk method due to a fluctuation, we developed a new estimation method based on stochastic process of neutron.

In this paper, a small reactivity worth measurement and its uncertainty estimation are described.

2. Methods and Results

In this section, some of the measurement techniques are described. This measurement technique is consisted of sample jerk method with a sample driving device and a reactivity meter. Additionally, we describe the results of critical experiment.

2.1 Sample jerk method

The sample jerk method is similar to pile oscillator or source jerk method. The procedure of sample jerk method is as follows:

1. An critical state with a sample,
2. Withdrawal of the sample from critical core,
3. Increase of the count rate of neutron detectors,
4. Measurement of reactivity worth with using the reactivity meter.

As shown above, the sample jerk method is not need a lot of procedure. The sample worth measurement can be carried out in a short time. Additionally, the sample jerk method is not need a sample oscillation. The experiment equipment can be miniaturized relative to

pile oscillator. For these reason, the sample jerk method is advantageous for reducing experimental costs and time for critical experiments

The specifications of the sample driving device are shown below:

- Maximum load : 5kg,
- Maximum withdrawal speed : 500mm/s,
- Maximum stroke : 1000mm.

2.2 Uncertainty estimation for reactivity fluctuation

The reactivity meter can be estimated by the inverse kinetic method (IK method)^[6] as shown following equation:

$$\rho = \beta + \frac{\Lambda}{n(t)} \frac{dn(t)}{dt} - \frac{\Lambda}{n(t)} \sum_m \lambda_m C_m(t). \quad (1)$$

The reactivity has a fluctuation due to stochastic process of neutron. As previously mentioned, it is important to accurately estimate the reactivity uncertainty.

There is a correlation among the fission sources between generations. Therefore, we have to evaluate the uncertainty with correlation.

A Monte Carlo code simulates a stochastic process of neutron like an actual phenomenon. Therefore, an estimation method of Monte Carlo code is valuable in evaluating the reactivity uncertainty. The MVP code^[7] uses Ueki method^[8] to evaluate the real variance of eigenvalue as shown following equation:

$$\sigma^2 = \frac{1}{N} \text{cov}[k_i, k_i] + \frac{2}{N} \sum_{i=1}^{N-1} \sum_{j=i+1}^N \text{cov}[k_i, k_j]. \quad (2)$$

The first term denotes a variance of i -th generation eigenvalue. The second term denotes a correlation of between generations. We apply Ueki method to evaluation the reactivity uncertainty as shown following equation:

$$\sigma^2 = \frac{1}{N} \text{cov}[\rho_i, \rho_i] + \frac{2}{N} \sum_{i=1}^{N-1} \sum_{j=i+1}^N \text{cov}[\rho_i, \rho_j]. \quad (3)$$

2.3 Experimental results

We carried out reactivity measurements by the sample jerk method in LWR-type critical facility, Toshiba Nuclear Critical Assembly (NCA). In these experiments, core consists of a uniform grid-plate, 2.0 wt% fuel rods and sample as shown Table 1. The sample is located in the center of core.

Table 1 Specification of experiments

Fuel rod pitch [cm]	1.52
Fuel enrichment[wt%]	2.0
Sample Material	Ni

We measured some times to confirm the reproducibility. The results of critical experiments are shown Table 2. The uncertainty results in Table 2 are estimated from the maximum difference of each experiment result. Eq.(3) is not used in this results. As shown Table2, the results of both methods are agreement within the experiment uncertainty. The uncertainty of sample jerk method is smaller than that of the deference of critical water level method, because the uncertainty of the critical water level has no effect on the measurement uncertainty of sample jerk method. Therefore, the sample jerk method is suitable for small sample worth.

Table 2 Confirmation of the reproducibility

Measurement method	Deference of critical water level	Sample jerk
Sample worth[¢]	3.73±0.40	3.77±0.10

An estimation of reactivity uncertainty is important to evaluate the sample worth in any measurement method. Figure 1 shows the reactivity of reactivity meter in a critical state. We estimate the uncertainty of reactivity by using Eq.(3) as shown Table 3. By considering the covariance, the uncertainty is increased three times. The influence of correlation is less than only 0.1 ¢. However, the influence becomes more important for small worth measurement. Therefore, this technique is useful for small worth measurement.

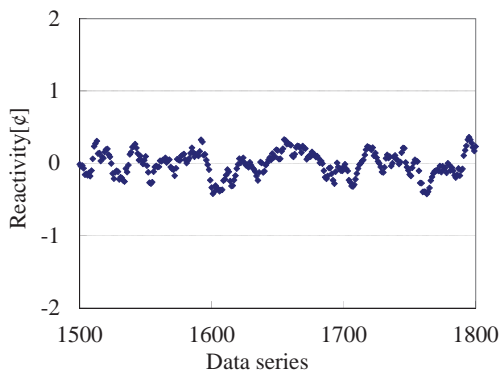


Fig. 1 Reactivity in critical state

Table 3 Estimation reactivity in critical state

Estimation method (Confidence interval:95%)	Not considering covariance	Considering covariance: Eq.(3)
Reactivity[¢]	-0.010±0.019	-0.010±0.061

* The uncertainties are variance of the average reactivity. Not variance of the each reactivity.

3. Conclusions

In this paper, we propose the sample jerk method for a small reactivity worth measurement and apply Ueki method to critical experiment. The sample jerk method is advantageous for reducing experimental costs and time for critical experiments

We carried out critical experiments for reactivity worth measurement in the deference of critical water level method and the sample jerk method. The result revealed that the sample jerk method can reduce the measurement uncertainty.

The Ueki method can consider the influence of correlation between neutron generations. We applied to the estimation of reactivity uncertainty for critical experiment. The influence of correlation is less than 0.1 ¢. However, the influence becomes more important for small worth measurement. Therefore, this technique is useful for small worth measurement.

As shown above, we propose the valuable method for small worth measurement in critical experiment.

REFERENCES

- [1] T. Kikuchi, K. Yoshioka, Y. Maru, Critical Experiments on Simulated BWR High-Burnup 9x9 A-Type Fuels, Proc. Physor96, Sep.16-20, 1996, Mito, Japan.
- [2] Y. Yamane, et. al., The Determination of Coupled-Core Reactor Kinetic Parameters Through Frequency Response, Nucl. Sci. Eng., Vol.76, pp.232-245, 1980.
- [3] S. Okajima, et. al., Analysis of Doppler Effect Measurement in FCA Cores Using JENDL-3.2 Library, Proc. Physor96, Sep.16-20, 1996, Mito, Japan.
- [4] K. Yoshioka, et. al., *Critical Experiments on Reduced-Moderation BWR:BARS – Reactivity Coefficients Measurements-*, ICAPP '03, May.4-7, 2003, Córdoba, Spain.
- [5] S. Gunji, et. al., Sample driving machine for reactor physics experiments – Application to sub-criticality measurement based on noise analysis-, AESJ2008, March.26-28, 2008, Osaka, Japan.
- [6] Z. Akcasu, et. al., *Mathematical Method in Nuclear Reactor Dynamics*, Academic Press, New York, p.88-97, 1971.
- [7] Y. Nagaya, et. al., MVP/GMVPII: General Purpose Monte Carlo Codes for Neutron and Photon Transport Calculations based on Continuous Energy and Multigroup Methods, JAERI-1348, 2005.
- [8] T. Ueki, et. al., Error Estimations and Their Biases in Monte Carlo Eigenvalue Calculations, Nucl. Sci. Eng., Vol.125, pp.1-11 1997.

A Neutronic Design of a Hybrid Reactor for Waste Transmutation

M. Tariq Siddique and Myung-Hyun Kim*

Department of Nuclear Engineering, Kyung Hee University, 446-701, Rep. of Korea
mhkim@khu.ac.kr

1. Introduction

A fusion-fission hybrid reactor concept is an attractive and efficient solution for burning of high level waste including transuranic (TRU) isotopes and fission products (FP). This study was initiated to explore the possibility of a hybrid reactor for transmutation of long-lived isotopes separated from PWR spent fuels [1] [2]. A concept of hybrid reactor for waste transmutation (Hyb-WT) is proposed which based on a low power Tokamak (less than 150 MWt) and annular ring shaped reactor core with multiple zones of metal fuel (TRU 60 w/o, Zr 40 w/o) and FP.

Performance of design concepts were measured by many indices such as TRU and FP mass burned per full power year, support ratio, reduction in TRU and FP toxicity and tritium breeding ratio. A variety of computational tools (codes) have been used for hybrid reactor design studies because of absence of specifically designed tool. MCNPX [3] and MONTEBURNS [4] codes are compared for the evaluation of Hyb-WT performance parameters. The differences among three most popular cross section libraries ENDF/B-VII, JEFF3.1.2 and JENDL3.2 are also evaluated.

2. Concept of Hyb-WT

The geometry and material composition of hybrid reactor for waste transmutation (Hyb-WT) are shown in Fig.1 and Table 1 respectively.

Table 1. Material composition of Hyb-WT

Zone	Material and volume fraction	Thickness (cm)
First Wall	ODS Steel (MA957): 70%, He-gas: 30%	5
TRU zone Vol % per Fuel Assembly	TRU: 3.56%, Zr: 7.04%, LiPb: 59.91%, SiC: 4.45%, Clad ODS steel: 9.98%, Na-Bond: 15.06%	45
FP zone	I-129: 0.5%, Cs-135: 1.7%, Tc- 99: 0.8%, SiC: 2.5%, C: 78%, He-gas: 16.5%	30

The Hyb-WT is based on a low power Tokamak (150 MW max) as a neutron source of fast neutrons. The geometrical parameters of Tokamak design are shown in table 2. The TRU core was designed at 2,000 MW_{th} fission power level [2] [5]. The material composition for TRU and FP are assumed to be same with those of spent fuel from 1,000 MW_e PWR with 10 years cooling time [6].

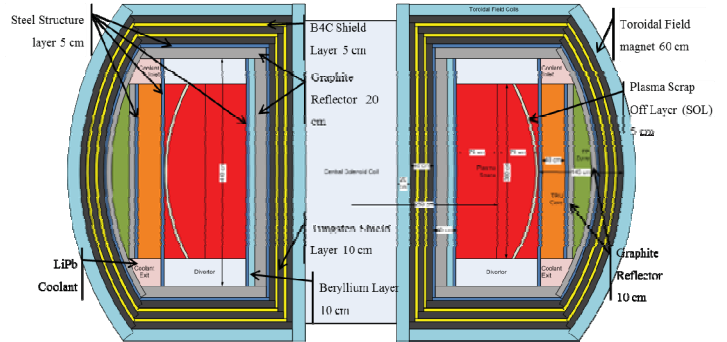


Fig. 1. Geometry of fusion-fission hybrid

Table 2. Geometrical parameters of Tokamak design.

Major radius R_0 (m)	3
Minor radius a (m)	0.7
Fusion Power P_{fus} (MW) max.	150
Neutron source ($\#/s^{-1}$) max.	6.7×10^{19}
Elongation κ	1.8
Triangularity δ	0.5
Aspect ratio	4.3
Plasma volume (m^3)	47.6

3. Comparison of MONTEBURNS and MCNPX

MONTEBURNS use one group cross sections [4] whereas MCNPX use 63 group cross sections [7] for depletion calculations which is the major difference between two code systems. To evaluate its effect on hybrid reactor design study depletion and toxicity variations of TRU and FP, k_{eff} and tritium breeding were calculated for Hyb-WT using MONTEBURNS and compared with MCNPX 2.6. ENDF/B-VII library was used for both codes.

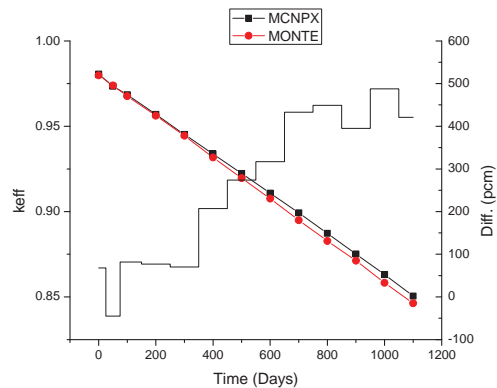


Fig. 2. Comparison of k_{eff} calculated with MCNPX and MONTEBURNS for Hyb-WT.

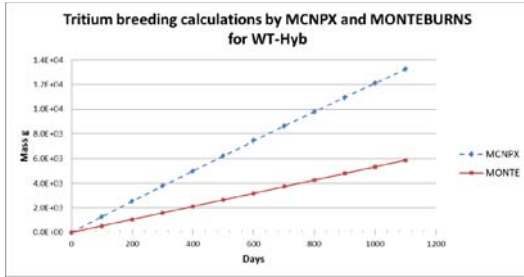


Fig. 3. Tritium breeding calculated by MCNPX and MONTEBURNS over the irradiation cycle for Hyb-WT.

The comparison of k-eff variation over the irradiation cycle for MONTEBURNS and MCNPX is shown in Fig. 2. The difference between two k-eff values is almost zero at the beginning of cycle and increased with time. The maximum difference was observed to be 488 pcm at the end of cycle. It shows that MONTEBURNS slightly overestimate the TRU transmutation.

There is very small difference in TRU mass depletion, the maximum % difference for TRU mass is 0.12% at the end of cycle and it also reflect slightly higher estimation of TRU transmutation by MONTEBURNS.

A big difference between MCNPX and MONTEBURNS tritium breeding calculation is observed as shown in Fig. 3. MCNPX calculates 13.24 kg tritium breeding whereas MONTEBURNS predicts 5.89 kg, over the irradiation cycle. It suggests that the data for Li-7 may not be considered for tritium breeding in MONTEBURNS as tritium production cross section for Li-7 is not negligible above 2 MeV.

4. Neutronic Analysis of Hyb-WT

Table 3 and 4 shows the summary of neutronic parameters and TRU and FP transmutation performance calculated using ENDF/B-VII, JEFF312 and JENDL32. The JEFF312 and JENDL32 resulted in overestimated k-eff values as compared to ENDF/B-VII even though similar TRU compositions and number densities are used. Because of different k-eff values the required fusion power and consequently the TBR is different for three libraries even though the tritium mass prediction by three libraries is not significantly different. The TRU transmutation performance of Hyb-WT predicted by three libraries is similar except the slight underestimation of TRU mass transmutation by JENDL32 but it significantly underestimates the FP transmutation.

Table 3: Major neutronic parameters of Hyb-WT predicted by ENDF/B-VII, JEFF312 and JENDL32 library.

Cross-section Library	ENDF/B-VII	JEFF312	JENDL32
Fusion Power (MW)	14-83	12-81	10-77
Range of k_{eff} variation	0.97133 - 0.85703	0.97606 - 0.86084	0.98071 - 0.86595
TBR	1.46	1.53	1.68
H3 Mass (kg)	11.67	11.59	11.86

Table 4: Transmutation performance parameters of Hyb-WT predicted by ENDF/B-VII, JEFF312 and JENDL32.

Neutron Library	TRU			FP		
	ENDF/B-VII	JEFF312	JENDL32	ENDF/B-VII	JEFF312	JENDL32
Inventory (T)	16.68	16.68	16.68	2.51	2.51	2.51
FP Mass Produced (kg)				162.85	162.89	162.83
Mass-burned (kg)	2250.4	2250.5	2249.7	251.55	254.51	222.67
(kg/fpy)	746.72	746.76	746.5	83.47	84.45	73.89
% mass-burned/yr	4.48%	4.48%	4.47%	3.32%	3.36%	2.94%
Support Ratio for 100% availability	2.99	2.99	2.99	2.09	2.12	1.85
Ingestion Toxicity Reduction	4%	4%	4%	11%	11%	11%
Inhalation Toxicity Reduction	8%	8%	8%	13%	13%	11%

5. Conclusions

MONTEBURNS may not be a better option for hybrid reactor design study especially for tritium breeding calculation. There is no significant difference between ENDF/B-VII and JEFF312 calculated performance parameters of Hyb-WT. JENDL32 shows significant difference from ENDF/B-VII for FP transmutation and k-eff value estimation. May be JENDL33 or JENDL4 calculations match closely with ENDF/B-VII because of improved cross section values.

The preliminary study of Hyb-WT shows great potential of fusion energy for waste transmutation. It is completely new and evolving technology it may require a comprehensive design and performance analysis over its life time which will be pursued for its practical application.

REFERENCES

- [1] M. T. Siddique and M.H. KIM, "Preliminary Neutronic Performance Evaluation on a Conceptual Design for a Transmutation Fusion Blanket," *Trans. Am. Nucl. Soc., Vol.105, 2011 ANS Winter Meeting, Washington D.C., USA, Oct.30-Nov.3, 2011.*
- [2] M. T. Siddique and M. H. KIM, "Preliminary Feasibility Study of a Low Power Hybrid Reactor," *Proc. of KSTAR conference, Muju Deogyusan Resort, Korea, Feb. 22-24, 2012.*
- [3] D. B. Pelowitz, "MCNPX User's Manual Version 2.6.0," *Los Alamos National Laboratory, 2008.*
- [4] R. Holly, I. David, and H. R. Trellue, "User's Manual, Version 2.0 for MONTEBURNS, Version 5B," 1999.
- [5] M. T. Siddique and M. H. Kim, "A Feasibility Study on a Clean Power Fusion Fission Hybrid Reactor," *Fusion Energy Conference 2012, San Diego, CA-USA, Oct. 8-13, 2012, pp. 1-8.*
- [6] H. Condé, "Introduction to ADS For Waste Incineration and Energy Production," *The Impact of Nuclear Science on Life Science, 2001.*
- [7] J. S. Hendricks, G. W. McKinney, M. L. Fensin, M. R. James, R. C. Johns, J. W. Durkee, J. P. Finch, D. B. Pelowitz, L. S. Waters, M. W. Johnson, and F. X. Gallmeier, "MCNPX 2.6.0 Extensions LA-UR-08-2216," 2008.

Two Formulations of Continuous-Energy Monte Carlo Local Problem in Overlapping Local/Global Iteration Methodology

YuGwon Jo and Nam Zin Cho*

Korea Advanced Institute of Science and Technology (KAIST)
291 Daehak-ro, Yuseong-gu, Daejeon, Korea 305-701

*nzcho@kaist.ac.kr

1. Introduction

The direct whole-core transport calculation without homogenization (in either multigroup deterministic or continuous-energy Monte Carlo method) is not yet tractable for routine use with current computing power. As an alternative to the direct approach, an overlapping local/global (OLG) iteration scheme [1, 2] was introduced, in which the local problem based on a multigroup deterministic method or a continuous-energy Monte Carlo method is embedded in the partial current-based coarse-mesh finite difference (p-CMFD) global problem.

As an illustration, Fig. 1 shows a half-assembly overlapping local problem (defined by green dot-dashed lines), to which the following neutron transport equation is applied:

$$\begin{aligned} \bar{\Omega} \cdot \nabla \varphi(\vec{r}, E, \bar{\Omega}) + \sigma_t(\vec{r}, E) \varphi(\vec{r}, E, \bar{\Omega}) = \\ \int d\bar{\Omega}' \int dE' \sigma_s(\vec{r}, E' \rightarrow E, \bar{\Omega}' \cdot \bar{\Omega}) \varphi(\vec{r}, E', \bar{\Omega}') + \\ \frac{1}{k^{local}} \frac{\chi(E)}{4\pi} \int d\bar{\Omega}' \int dE' \nu \sigma_f(\vec{r}, E') \varphi(\vec{r}, E', \bar{\Omega}'). \end{aligned} \quad (1)$$

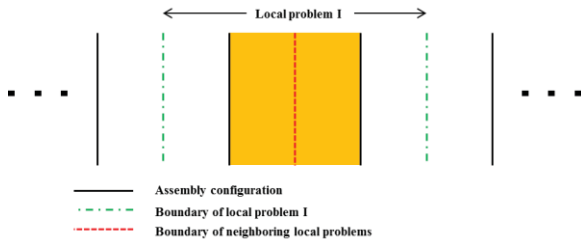


Fig.1. Half-assembly overlapping local problem in 1-D problem

From a global solution in the OLG iteration scheme, (i) φ^\pm or J^\pm at the local problem boundary and (ii) k^{global} become available at each iteration. In Ref. [1], in the case of deterministic local problem, a fixed-source problem formulation is used in that $\varphi^{BC} = \varphi^-$ and $k^{local} = k^{global}$ are used to solve Eq. (1). This may be also termed as a “fixed-k problem (FKP)” formulation with incoming angular flux boundary condition.

In the case of continuous-energy Monte Carlo local problem, Refs. [1] and [2] describe an eigenvalue problem (EVP) formulation with albedo boundary condition $\alpha = J^-/J^+$ given, but k^{local} is unknown. As another formulation, this paper presents a fixed-k

problem (FKP) formulation and compares the two formulations.

2. Two Formulations of Continuous-Energy Monte Carlo Local Problem

2.1 Eigenvalue Problem (EVP) with Albedo Boundary Condition [1, 2]

When a Monte Carlo particle is about to cross a boundary surface, it is reflected with a new weight corrected by albedo α . This is enabled by the “albedo-to-weight” conversion device developed in a Monte Carlo depletion study [3], and it is almost trivial to implement the method in an existing Monte Carlo code.

2.2 Fixed-k Problem (FKP) with Incoming Partial Current Boundary Condition

In this problem formulation, incoming partial current $J^{BC} = J^-$ (in angular bins) and $k^{local} = k^{global}$ are given from the previous local/global iteration. In each generation j , we consider N histories such that

$$N = N_j^s + N_j^f, \quad j = 1, 2, \dots, \quad (2)$$

where N is user input, N_j^s is the number of histories sampled from the incoming boundary source and N_j^f is the number of histories taken from the fission source banked in generation $j-1$ and obtained as

$$N_j^f = \sum_{i=1}^{N_{j-1}^s + N_{j-1}^f} \left(\sum_{col} \left(\text{floor} \left(\frac{\nu \sigma_f / \sigma_t}{k^{global}} \text{wgt}_{i,col} + \xi \right) \right) \right), \quad (3)$$

$$N_j^s = N - N_j^f. \quad (4)$$

Note that $\nu \sigma_f$ is divided by k^{global} in Eq. (3).

After several generations are discarded, the subnode p-CMFD parameters [1, 2] are tallied based on collision estimators for next global calculation.

3. Numerical Results

The two formulations of continuous-energy Monte Carlo local problem in the OLG methodology are tested and their performances are compared in the 1-D thermal reactor problem [1] shown in Fig. 2. The Monte Carlo calculations are performed by the in-house research code McSLAB [4], which considers at the present time three major interactions (elastic scattering, capture,

fission) with resolved resonances and isotropic scattering in the center-of-mass system taken into account.

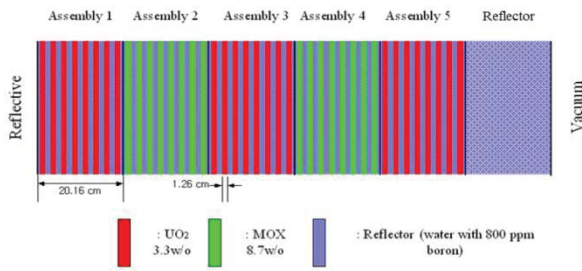


Fig.2. 1-D thermal reactor with UO₂ and MOX fuel assemblies

To render the longest running time among local problems similar in the two formulations, 5×10^4 histories for EVP and 6.5×10^4 histories for FKP per generation are selected and 50/500 inactive/active generations are used for each local calculation. Homogenized parameters are generated in two groups for global subnode p-CMFD calculation, while boundary conditions for local problems are modulated in 45 energy groups and four angular bin partial currents. For the reference whole-core calculation, 2.5×10^5 histories per generation and 200/3000 inactive/active generations are used.

Table I shows the computing times of local problems in the two formulations at the 6-th OLG iteration. Note that in EVP the Monte Carlo particle is reflected at a boundary surface (with adjusted weight) and tracked further until it is absorbed, while in FKP the particle is not tracked further when it crosses such a surface.

Table I. Computing times (min, Intel Xeon X5670 single processor running at 2.93 GHz) of local problems at the 6-th OLG iteration

Local Problem	1	2	3	4	5	6
FKP	78.63	62.56	68.00	63.32	69.75	48.92
EVP	70.89	73.90	73.92	74.45	77.77	73.28

As the OLG iteration progresses, k^{global} and relative root mean square errors (rRMSE) of subnode averaged power distributions of the two formulations are compared in Figs. 3 and 4, respectively.

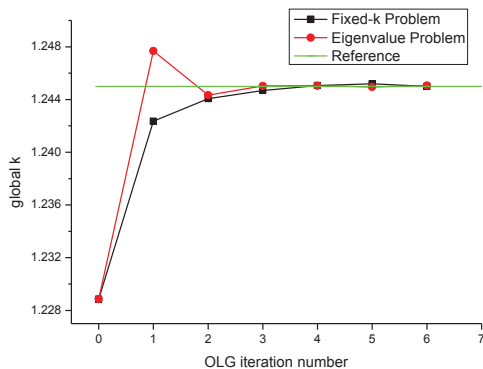


Fig.3. Comparison of global k's in two formulations

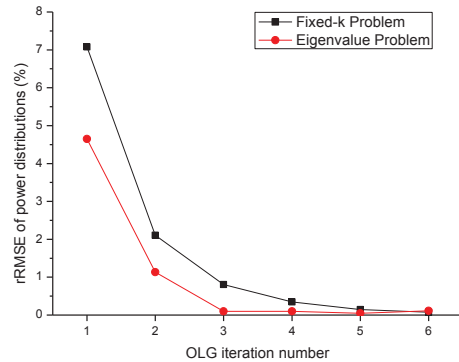


Fig.4. Comparison of rRMSEs of subnode averaged power distributions in two formulations

4. Conclusions

In addition to the eigenvalue problem (EVP) formulation, this paper describes the fixed-k problem (FKP) formulation of the continuous-energy Monte Carlo local problem to be embedded in the overlapping local/global (OLG) iteration methodology. The two formulations are tested on a simplified but typical thermal reactor problem. The test results indicate that the rRMSEs of power distributions converge faster in EVP than in FKP, when the maximum computing times for local calculations are similar.

In contrast to EVP, the computing times in FKP vary widely among local problems, depending on the local problem characteristics and its environment. Therefore, it will be difficult to achieve good load balance in parallel computation of local problems with FKP.

References

1. N.Z. Cho et al., "Overlapping Local/Global Iteration Framework for Whole-Core Transport Solution," PHYSOR 2012, Knoxville, TN, USA (2012); see also *Nucl. Sci. Eng.*, accepted (2013).
2. Y.G. Jo and N.Z. Cho, "Refinement of Overlapping Local/Global Iteration Method Based on Monte Carlo/p-CMFD Calculations," M&C 2013, Sun Valley, ID, submitted (2013).
3. S. Yun and N.Z. Cho, "Monte Carlo Depletion under Leakage-Corrected Critical Spectrum via Albedo Search," *Nucl. Eng. Technol.*, Vol.42, p.271 (2010); <http://www.kns.org/jknsfile/v42/JK0420271.pdf>.
4. Y.G. Jo, "McSLAB – A Continuous-Energy Monte Carlo Code for Neutronics Analysis in Multi-Slab Geometry," Korea Advanced Institute of Science and Technology (KAIST), in progress.

Efficient Calculation Scheme with Preservation of Transmission Probabilities in the Method of Characteristics

Masato Tabuchi^{a,b,*}, Naoki Sugimura^a, Akio Yamamoto^b, Tomohiro Endo^b
^a*Nuclear Engineering Ltd., Tosabori Nishi-ku, Osaka, Japan, 550-0001*
^b*Nagoya University, Furo-cho, Chikusa-ku, Nagoya-shi, Aichi, Japan, 464-8603*
^{*}*Corresponding author: mtabuchi@neltd.co.jp*

1. Introduction

In the method of characteristics (MOC) [1], parameters for the ray tracing, which mean azimuthal angle division, polar angle division and ray separation width, are important in the viewpoint of computational burden and accuracy. Although faster calculation can be performed with coarser ray tracing parameters, accuracy would be degraded because of the discretization error. In particular, for a strong absorber cell such as high Pu content MOX, very detailed ray tracing is required to obtain an accurate result. In order to improve the calculation efficiency, in this study, an efficient calculation scheme to reduce discretization error due to the ray separation is discussed.

2. Calculation Model

In most of the ordinary MOC calculation codes, equidistant ray tracing is used. However, in this approach, a ray trace may cover geometrical discontinuous points, e.g. intersects of regions, hence large discretization error would be caused in such situation. In order to avoid this issue, the macroband method was developed in the previous study [2, 3]. In the macroband method, a calculation domain is divided into “macroband”, boundaries of which consists of tangential and intersect points in the calculation geometry. Then each macroband is divided into “segment” and the path lines are drawn at the center of the segments. The discretization error due to the ray separation is expected to be reduced, since no segments include discontinuous points with the macroband method. Moreover, in the AEGIS code [4], non-equidistant ray tracing in each macroband based on the Gauss-Legendre quadrature set is adopted to reduce numerical integration error. In this study, the improvement of the ray tracing is discussed by another aspect. The present study focuses on preservation of the transmission probabilities in each segment. The transmission probability is an important parameter, since it represents the effective neutron attenuation. However, it is difficult to generally and rigorously estimate the transmission probability, since the probability depends on not only the total cross section but also geometrical shape of a segment. In order to easily estimate the transmission probability, in this study, length distribution of path lines in a segment is assumed to obey a linear function. For the derivation of

the present model, the macroband method based on the equidistant ray tracing is assumed.

The equation for preservation of the transmission probability in a segment is described as follows:

$$\alpha = \frac{\Sigma_t}{\sin \theta} \quad (1)$$

$$\int_{-1}^1 \exp(-\alpha s(t)) dt = 2 \exp(-\alpha \tilde{s}) \quad (2)$$

In Eq. (2), the coordinate system in a segment, which is normal to the direction of ray trace, is normalized as -1 to 1. An example of the length distribution of path lines, which means $s(t)$ in Eq. (2), is shown in Fig. 1.

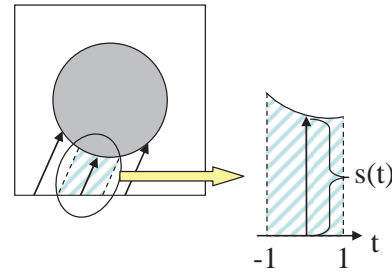


Fig. 1. An example of the length distribution

When the length distribution of path lines is assumed to be a linear function as shown in Eq. (3), the effective length to preserve the transmission probability can be obtained as Eq. (4):

$$s(t) = \beta t + \gamma \quad (3)$$

$$\tilde{s} = \gamma - \frac{1}{\alpha} \ln \left(\frac{1}{\alpha \beta} \sinh(\alpha \beta) \right) \quad (4)$$

Furthermore, using a special function defined as Eq. (5), Eq. (4) can be rewritten as Eq. (6):

$$L(x) = \frac{1}{x} \ln \left(\frac{1}{x} \sinh(x) \right) \quad (5)$$

$$\tilde{s} = \gamma - \beta L(\alpha \beta) \quad (6)$$

Since $L(x)$ is the odd function ($L(-x) = -L(x)$), the following relationship is satisfied:

$$\gamma - (-\beta)L(-\alpha\beta) = \gamma - \beta L(\alpha\beta) \quad (7)$$

Therefore, only the absolute value of β should be considered, and $L(x)$ can be considered only in the range of positive x . Fig. 2 shows the distribution of $L(x)$ for positive x . As shown in Fig. 2, $L(x)$ is a monotonically increasing function, and the range of its values is between 0 and 1.

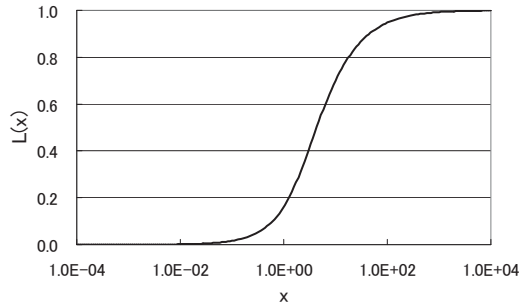


Fig. 2. Distribution of $L(x)$ for positive x

As described above, the effective length to preserve the transmission probability can be obtained by Eq. (6). The first term of the right hand side of Eq. (6) is equivalent to the average length of a segment, since \mathcal{Y} represents the intercept of the length distribution and the coordinate system in a segment is normalized as -1 to 1. The second term of the right hand side of Eq. (6) consists of a multiplication of β and $L(x)$, which can be both regarded as positive values. Therefore, the effective length always becomes shorter than the average length of a segment to preserve the transmission probability.

In the actual implementation, α , β , \mathcal{Y} and $L(x)$ should be estimated to obtain the effective length. Although α can be estimated before the transport sweep, a large amount of memory would be necessary in some cases. Therefore, α should be estimated during the transport sweep. On the other hand, if β and \mathcal{Y} are estimated during the transport sweep, additional calculation cost would be significantly increased. Therefore, these values should be estimated before the transport sweep. These values can be easily estimated by drawing some additional lines in a segment during the ray tracing. Finally, $L(x)$ should be tabulated before the transport sweep, since $L(x)$ includes logarithm and hyperbolic sine functions, which need much computational time to be calculated. By adopting the above scheme, the calculation model of the present study can be implemented without significant additional cost, and the efficiency of the MOC calculation is expected to be improved.

3. Verification

In order to confirm the accuracy of the present method, some verification calculations are performed. As the conventional method, the macroband method based on the Gauss-Legendre quadrature set, which is explained in the first paragraph, is assumed, and the accuracy is compared between the conventional and the present methods. Four types of 17 x 17 fuel assemblies listed as follows are assumed for the verification, and k-infinity values are evaluated by the AEGIS code.

- 4.8 wt% UO₂ fuel ('UO2')
- 4.8 wt% UO₂ fuel with RCC insertion ('RCC')
- 10.0 wt% Gd bearing 4.8 wt% UO₂ fuel ('GD')
- 4.0, 8.0, 12.0 wt% Pu-total MOX fuel ('MOX')

In this verification, these geometries are called as 'UO2', 'RCC', 'GD' and 'MOX' respectively. The calculation conditions are as follows. In order to evaluate the discretization error due to the ray separation, divisions for azimuthal and polar angles are set to be detail.

- Energy group: 172 groups (XMAS structure [5])
- Azimuthal angle division: 128 for 2π
- Polar angle division: 3 for $\pi/2$ (TY-quadrature [6])
- Ray separation width: vary between 0.01 and 0.35 cm
- Scattering order: P0 (transport correction)

It should be noted that the actual ray separation widths are different from the input values, since widths of macrobands are different from each other. Therefore, input value means the maximum ray separation width. The above condition of the ray separation widths (0.01 to 0.35 cm in input values) corresponds to about 0.01 to 0.12 cm in average ray separation widths.

The calculation results are shown in Figs. 3 to 6. These figures show the trends of k-infinity differences against the ray separation. The results in the conventional method with 0.01 cm width are used as the reference results. As described above, the actual ray separation widths are not equal to the input values. Therefore, the average ray separation width is used as the horizontal axis in Figs. 3 to 6.

In the conventional method, the differences of k-infinity become larger when the ray separation widths become coarser. The maximum difference is more than 0.1 % $\Delta k/k$, and the trends of the differences have oscillation-like behaviors in some cases. On the contrary, in the present method, although the differences become slightly larger for coarser ray separation width, the maximum difference is smaller than 0.05 % $\Delta k/k$. Furthermore, the oscillation-like behaviors in the present method are not remarkable compared with those in the conventional method.

From these results, the effectiveness of the present method can be confirmed. Since the accuracy is not

greatly decreased for coarse ray separation width in the present method, efficiency of the MOC calculation is expected to be improved by the present method.

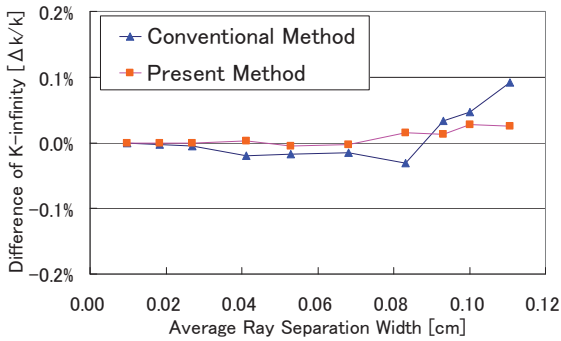


Fig. 3. Verification results for UO2

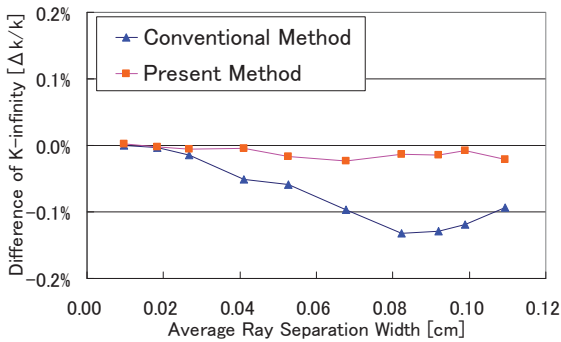


Fig. 4. Verification results for RCC

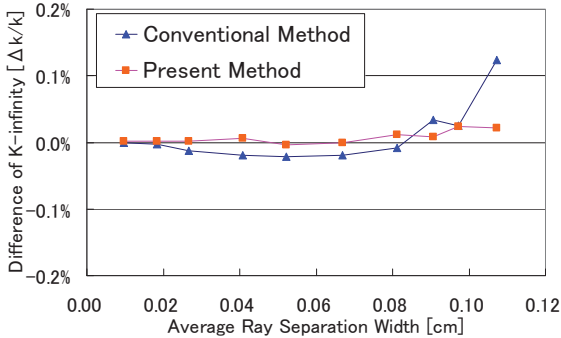


Fig. 5. Verification results for GD

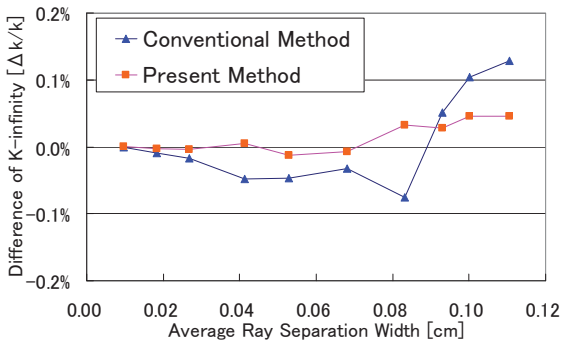


Fig. 6. Verification results for MOX

4. Summary

In this study, an efficient calculation scheme for MOC is investigated. The equation for the effective length of a path line is derived based on an assumption that the lengths are linearly distributed in a segment. By using the effective length, the transmission probabilities in each segment can be preserved. Through the verification calculations, the accuracy of the present method can be confirmed, and efficiency of the MOC calculation is expected to be improved by the present method.

REFERENCES

- [1] J. R. ASKEW, A Characteristics Formulation of the Neutron Transport Equation in Complicated Geometries, AEEW-M 1108, U. K. Atomic Energy Authority, 1972.
- [2] E. A. Villarino, R. J. J. Stammler, A. A. Ferri, J. J. Casal, HELIOS: Angularly Dependent Collision Probabilities, Nuclear Science and Engineering, Vol.112, p.16, 1992.
- [3] T. Ushio, T. Takeda, M. Mori, Neutron Anisotropic Scattering Effect in Heterogeneous Cell Calculations of Light Water Reactors, Journal of Nuclear Science and Technology, Vol.40, p.464, 2003.
- [4] A. Yamamoto, T. Endo, M. Tabuchi, N. Sugimura, T. Ushio, M. Mori, M. Tatsumi, Y. Ohoka, AEGIS: an advanced lattice physics code for light water reactor analyses, Nuclear Engineering and Technology, Vol.42, p.500, 2010.
- [5] E. Sartori, Standard Energy Group Structures Of Cross Section Libraries For Reactor Shielding, Reactor Cell and Fusion Neutronics Applications: VITAMIN-J, ECCO-33, ECCO-2000 and XMAS, JEF/DOC-315, Revision 3, NEA, Data Bank, Gif-sur-Yvette Cedex, France, Dec. 11, 1990.
- [6] A. Yamamoto, M. Tabuchi, N. Sugimura, T. Ushio, M. Mori, Derivation of optimum polar angle quadrature set for the method of characteristics based on approximation error for the Bickley function, Journal of Nuclear Science and Technology, Vol.44, p.129, 2007.

Hybrid Method of MOC and MC for Efficient Neutron Transport Analysis

Deokjung Lee* and Hyunsuk Lee
Ulsan National Institute of Science and Technology
 *Corresponding author: deokjung@unist.ac.kr

1. Introduction

For the neutron transport analysis, two approaches have been developed independently for several decades: deterministic and probabilistic approaches. Recently, there are efforts to combine these two approaches to take advantage of the two. Kim et al. used the Monte Carlo (MC) method inside an Method of Characteristics (MOC) code to generate on-the-fly multi-group shielded data for the resonance region [1]. Lee et al. used coarse mesh finite difference method (CMFD) to accelerate the MC calculation [2]. Williams et al. used a hybrid approach of multi-group and continuous-energy which computes problem-specific continuous-energy neutron spectra in the resonance energy region and uses that spectra to process resonance-shielded multi-group data for downstream transport calculations [3]. Larsen and Yang used MC as a generator of functionals for the low order deterministic operators [4]. But none of these efforts is a direct coupling of the two approaches. Lee proposed a hybrid method directly coupling the MOC and MC within a framework of multigroup transport [5]. This paper present the extension of Lee's method to continuous energy neutron transport, which uses MOC for high and low energies and MC for resonances.

2. Methods and Results

In this section, the MOC, MC and hybrid methods will be described briefly.

2.1 Method of Characteristics

The Boltzmann neutron transport equation can be written as:

$$\begin{aligned} \mathbf{\Omega} \cdot \nabla \varphi(\mathbf{r}, E, \mathbf{\Omega}) + \Sigma_t(\mathbf{r}, E) \varphi(\mathbf{r}, E, \mathbf{\Omega}), \\ = q(\mathbf{r}, E, \mathbf{\Omega}) \end{aligned} \quad (1)$$

where the source term $q(\mathbf{r}, E, \mathbf{\Omega})$ includes fission source and scattering source. After integration over energy and space, Eq. (1) can be rewritten as below for a direction m :

$$\frac{d\varphi_{m,i}^g}{ds_m} + \Sigma_{t,i}^g \varphi_{m,i}^g = Q_{m,i}^g. \quad (2)$$

This equation can be solved analytically with the assumption of flat source in each computational mesh. The scalar fluxes and eigenvalues can be evaluated using power method.

2.2 Monte Carlo Method

The MC simulation of the Eq. (1) can be written as below:

$$\begin{aligned} \Psi(\mathbf{r}, E, \mathbf{\Omega}) = \\ \left[\int \int \int C(\mathbf{r}', E' \rightarrow E, \mathbf{\Omega}' \rightarrow \mathbf{\Omega}) dE' d\mathbf{\Omega}' \right. \\ \left. + Q(\mathbf{r}', E, \mathbf{\Omega}) \right] \\ \times T(\mathbf{r}' \rightarrow \mathbf{r}, E, \mathbf{\Omega}) d\mathbf{r}' \end{aligned} \quad (3)$$

where $\Psi(\mathbf{r}, E, \mathbf{\Omega})$ is the particle collision density, $C(\mathbf{r}', E' \rightarrow E, \mathbf{\Omega}' \rightarrow \mathbf{\Omega})$ is the collision kernel, and $T(\mathbf{r}' \rightarrow \mathbf{r}, E, \mathbf{\Omega})$ is the transport kernel. Eigenvalues and fluxes can be tallied either collision estimator or track length estimator.

2.3 Hybrid Method

Hybrid method uses MOC and MC together in the solution process of Boltzmann transport equation. The approach in this paper is to use MOC for high and low neutron energy groups and MC for intermediate resonance energy range with continuous energy cross sections. The group sweeping order in the hybrid method is from the highest energy group ($g=1$) to the lowest energy group ($g=ng$) where ng is the total number of groups. The groups for MC simulation are from gb to ge . The source term in the hybrid can be written as:

$$\begin{aligned} Q_i^g = \sum_{g'=1}^{gb-1} \sum_{s,i}^{g' \rightarrow g} \phi_i^{g'} \\ + \frac{\chi^g}{k_\infty} \left[\sum_{g'=1}^{gb-1} \nu \Sigma_f^{g'} \phi_i^{g'} + \sum_{g'=gb}^{ge} \nu \Sigma_f^{g'} \bar{\phi}_i^{MC, g'} \right], \quad (4) \\ g = gb, \dots, ge \end{aligned}$$

where $\bar{\phi}_i^{MC, g'}$ is the mesh average flux calculated from the MC simulation.

The MC simulation in the hybrid method is a fixed source problem using the source in the above equation. The sites of source neutrons are sampled uniformly in each cell and the total number of source neutrons, n_i^g , in cell i , group g , is proportional to the source from the high energy MOC groups, *i.e.*,

$$n_i^g = n_i^{g,s} + n_i^{g,f} \quad (5)$$

$$= \sum_{g'=1}^{gb-1} N \times p_i^{g' \rightarrow g,s} + N \times p_i^{g,f}$$

where $n_i^{g,s}$ and $n_i^{g,f}$ are scattering source from higher groups and fission source from previous cycle, respectively, N is the total number of starting neutrons in each cycle, and $p_i^{g' \rightarrow g,s}$ is the fraction of the neutron source from group g' to group g , in cell i .

2.4 Numerical Test

A model pin cell problem is designed to test the proposed method. Figure 1 shows the model problem geometry with fuel, clad, and coolant regions. The coolant region is subdivided into two calculation meshes in the radial direction for MOC. The boundary conditions are all reflective.

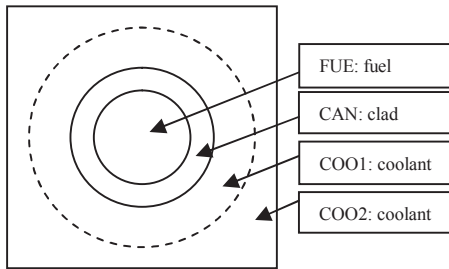


Fig. 1. Model problem geometry

Figure 2 shows the power iterations of hybrid method. It is interesting to note that the eigenvalue behavior is similar to that of MC simulation, i.e., fluctuations due to the MC for the resonance energy range which requires statistical treatment of the solutions. The average of keff values is plotted in red to show the converging behavior.

The eigenvalues of five different calculations are summarized in Table II: two MC solutions, one MOC solution, and two hybrid solutions. The first MC solution is the reference for comparison. The numbers of inactive cycles, active cycles, and histories per cycle are 50, 1000, and 100000, respectively as shown in the second column. The difference of MC solution and MOC can be attributed to the error in the multi group cross-section calculated from a continuous MC simulation. For the two hybrid method solutions, the numbers of active cycle, histories and iterations are 10/1000/600 and 10/10000/600, respectively. The table shows that the hybrid method can produce consistent solutions with the reference MC solutions and MOC solutions.

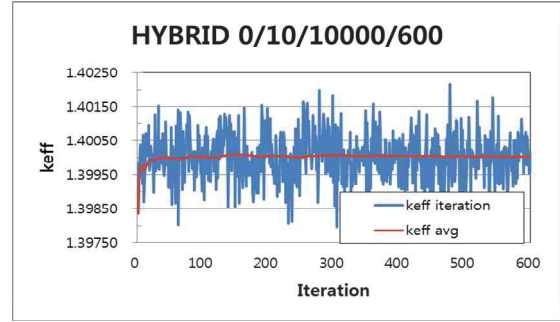


Fig. 2. Hybrid simulation.

Table I: Summary of Eigenvalues

Method	Inactive/ active/ history/ iteration	keff	Standard deviation	Error(pcm)
MC	50/1000/ 100000/0	1.39971	0.00009	(Reference)
MC	50/1000/2000/0	1.39953	0.00068	18
MOC	0/0/0/247	1.39801	-	170
HYBRID	0/10/1000/600	1.40012	0.00084	-41
HYBRID	0/10/10000/600	1.40004	0.00026	-33

3. Conclusions

This paper presents the hybrid method of deterministic and probabilistic approaches applied to a continuous energy transport model problem, which is an extension of the multi-group hybrid method proposed by Lee [5]. Continuous energy cross sections are directly used in the MC calculation for the resonance energy range and multi-group cross sections are used in the MOC calculations for the fast and thermal energy groups. In terms of eigenvalues and cell average fluxes, the hybrid method show consistent results with the reference MC-only calculations as well as MOC-only calculations. The future work will be the optimization of the hybrid method to improve the computational performance.

ACKNOWLEDGMENTS

This research was supported by National Nuclear R&D Program through the National Research Foundation of Korea (NRF) funded by the Ministry of Education, Science and Technology.

REFERENCES

- [1] Kang-Seog Kim, et al., "Monte Carlo Resonance Treatment for the Deterministic Transport Lattice Codes," *Journal of the Korean Nuclear Society*, **35**, pp. 581-595, 2003
- [2] Min Jae Lee, Han Gyu Joo, Deokjung Lee, and Kord Smit h, "Multigroup Monte Carlo Reactor Calculation with Coarse Mesh Finite Difference Formulation for Real Variance Reduction," *Proc. SNA+MC2010*, October 17-21, Tokyo, Japan, 2010

- [3] M. L. Williams, M. Asgari, D. F. Hollenbach, "CENTRM: A ONE-DIMENSIONAL NEUTRON TRANSPORT CODE FOR COMPUTING POINTWISE ENERGY SPECTRA," ORNL/TM-2005/39 , Version 6, Vol. II, Sect. F18
- [4] Edward W. Larsen and Jinan Yang, "A Functional Monte Carlo Method for k-Eigenvalue Problems," Nucl. Sci. Eng., 159, pp. 107-126 2008
- [5] Deokjung Lee, "HYBRID METHOD OF DETERMINISTIC AND PROBABILISTIC APPROACHES FOR MULTIGROUP NEUTRON TRANSPORT PROBLEM," PHYSOR 2012, Knoxville, Tennessee, USA, 2012